

AperTO - Archivio Istituzionale Open Access dell'Università di Torino

Mutations in NOTCH1 PEST-domain orchestrate CCL19-driven homing of Chronic Lymphocytic Leukemia cells by modulating the tumor suppressor gene DUSP22

This is a pre print version of the following article:

Original Citation:

Availability:

This version is available <http://hdl.handle.net/2318/1621657> since 2022-05-12T16:35:34Z

Published version:

DOI:10.1038/leu.2016.383

Terms of use:

Open Access

Anyone can freely access the full text of works made available as "Open Access". Works made available under a Creative Commons license can be used according to the terms and conditions of said license. Use of all other works requires consent of the right holder (author or publisher) if not exempted from copyright protection by the applicable law.

(Article begins on next page)

Title: Mutations in *NOTCH1* PEST domain orchestrate CCL19-driven homing of leukemic cells by modulating the tumor suppressor gene *DUSP22*

Authors: Francesca Arruga^{1,2}, Branimir Gizdic^{1,2}, Cinzia Bologna^{1,2}, Simona Cignetto^{1,2}, Roberta Buonincontri^{1,2}, Sara Serra^{1,2}, Tiziana Vaisitti^{1,2}, Katiuscia Gizzi¹, Nicoletta Vitale³, Giulia Garaffo³, Elisabetta Mereu³, Fary Diop⁴, Francesco Neri¹, Marta Coscia³, John Allan⁶, Roberto Piva³, Salvatore Oliviero^{1,5}, Richard R. Furman⁶, Davide Rossi⁴, Gianluca Gaidano⁴, Silvia Deaglio^{1,2}.

Affiliations: ¹Human Genetics Foundation, Torino, Italy; ²Department of Medical Sciences, ³Department of Molecular Biotechnologies and Health Science and ⁵Department of Life Sciences and Systems Biology, all at the University of Turin; ⁴Division of Hematology, Department of Translational Medicine, University of Eastern Piedmont, Novara, Italy; ⁶Department of Hematology, Weill Cornell Medicine, New York, NY.

Contact: Silvia Deaglio, MD, PhD, Department of Medical Sciences, University of Torino School of Medicine & Human Genetics Foundation (HuGeF), via Nizza, 52, 10126 Torino, Italy. Email: silvia.deaglio@unito.it or silvia.deaglio@hugef-torino.org.

Abstract

Even if *NOTCH1* is commonly mutated in Chronic Lymphocytic Leukemia (CLL), its functional impact in the disease remains unclear. Using CRISPR/Cas9-generated cell models, we show that NOTCH1 regulates growth and homing of CLL cells by dictating expression levels of the tumor suppressor gene *DUSP22*. Specifically, NOTCH1 affects the methylation of *DUSP22* promoter by modulating a nuclear complex, which tunes the activity of DNA methyltransferase 3A (DNMT3A). These effects are enhanced by PEST-domain mutations, which stabilize the molecule and prolong signaling. CLL patients with a *NOTCH1*-mutated clone showed low levels of *DUSP22* and active chemotaxis to CCL19. Lastly, in xenograft models, *NOTCH1*-mutated cells displayed a unique homing behavior, localizing preferentially to the spleen and brain. These findings connect NOTCH1, *DUSP22*, and CCL19-driven chemotaxis within a single functional network, suggesting that modulation of the homing process may provide a relevant contribution to the unfavorable prognosis associated with *NOTCH1* mutations in CLL.

Introduction

Exome sequencing identified previously unrecognized, recurrently mutated genes in CLL. *NOTCH1* mutations are found in $\approx 10\%$ of CLL patients at diagnosis, with the prevalence increasing to $\approx 20\%$ in relapsed patients, and to $\approx 30\%$ in the subset that undergoes transformation to Richter's syndrome (RS) (1-4). Several studies report strong associations between *NOTCH1* mutations and unmutated immunoglobulin V genes (IgHV), stereotyped B cell receptors typical of subset #8, trisomy 12, and an increased risk of RS (5-10). Furthermore, patients with *NOTCH1* mutations have a shorter time to first treatment and reduced overall survival, independent of other prognostic indicators (7, 11). The impact of *NOTCH1* mutations as drivers of clonal evolution in CLL remains unclear. However, *NOTCH1* mutations occur early in the disease process, since they are found in patients with monoclonal B cell lymphocytosis (12, 13) as well as in patients with RS (14).

In a significant proportion of cases, *NOTCH1* mutations in CLL are represented by a 2bp frameshift deletion mutation at position 7541-7542 (Δ CT_7541-7542), leading to the formation of a premature STOP codon, resulting in a shorter protein. The protein lacks the ubiquitination site and is thus predicted to remain transcriptionally active in the nucleus for a longer time.

In a prior comparison of *NOTCH1* expression and signaling in CLL patients carrying WT or Δ CT_7541-7542 mutation, we showed that mutated patients are characterized by increased expression of *NOTCH1* targets, such as *HES1* and *DTX1*, which are prototypes of the canonical and non-canonical pathway. We also showed that, regardless of

mutational status, NOTCH1 signaling must be activated through interactions with the surface ligands (15). From a functional perspective, *NOTCH1* mutations render CLL cells more resistant to spontaneous or drug-induced apoptosis (16, 17).

Binding to ligands belonging to the Jagged or DLL families starts multiple proteolytic cleavages of the NOTCH1 protein, the last of which is operated by the γ -secretase enzyme, causing nuclear translocation of the NOTCH1-IntraCellular-Domain (NICD) (18). Once in the nucleus, the NICD forms a transcription complex with the DNA binding protein RBPJk and other co-activators (19). The presence of the more stable, mutant, form of NICD is predicted to alter the nuclear balance between RBPJk, the NICD itself, and histone deacetylase 1 (HDAC1) which also binds to RBPJk (20).

Here, by using a cellular model lacking *NOTCH1* or expressing it in a WT or mutant form, we show that NOTCH1 modulates the expression of molecules involved in signaling and movement. We highlight a novel nuclear circuit, which connects the NICD to the activity of the DNMT3A, through RBPJk and HDAC1. This circuit modulates methylation and subsequent expression of the tumor suppressor DUSP22, which in turn negatively regulates activation of the MAP kinases (MAPK) and STAT3 signaling.

Results

***NOTCH1*-deficient Mec-1 cells are generated using CRISPR technology and reconstituted using lentiviruses encoding WT or mutant NICD**

To address the role of NOTCH1 in CLL homeostasis, we exploited the CLL-derived Mec-1 cell line, which constitutively expresses wild-type (WT) NOTCH1 at high levels (Fig. 1A-B). By using CRISPR/Cas9 technology targeted to exon 2 of the gene, we generated a Mec-1 variant lacking NOTCH1 (Mec-1/KO) (fig. S1A). Transfected cells were then sorted for GFP and cloned by limiting dilution. The clones were screened by Sanger sequencing to check for missense mutations in the area targeted by the guide (fig. S1B). Lack of NOTCH1 expression was confirmed by qRT-PCR and western blot (WB) (Fig. 1A-B). Three different clones constitutively lacking NOTCH1 were used for further studies.

To elucidate the role of the mutations in the *NOTCH1* PEST domain, which are typical of CLL patients, Mec-1/KO cells were infected with GFP-tagged lentiviruses encoding either WT or mutant NICD, designated KO^{NICD} and KO^{NICD-M}, respectively. The mutant NICD was generated by site-specific mutagenesis to obtain the Δ CT_7541-7542 mutation. Expression of WT or mutant NICD was confirmed by WB, which showed multiple bands corresponding to the NICD (Fig. 1A). As expected, the presence of the mutation resulted in bands of lower molecular weight, compatible with the appearance of a premature STOP codon. By immunoprecipitation (IP) with an anti-NOTCH1 antibody, we confirmed that these molecular species react with an anti-NOTCH1 antibody (fig. S2). qRT-PCR showed that NOTCH1 expression in the infected cells was comparable to that of Mec-1/WT (Fig. 1B).

Expression of NOTCH1-dependent genes was then studied by RT-PCR in at least three different KO, KO^{NICD}, and KO^{NICD-M} clones, the latter two selected for expressing comparable levels of NOTCH1. Loss of NOTCH1 expression was followed by a drop in the expression of *HES1* and *DTX1* (Fig. 1C-D), which was restored by reconstitution of a transcriptionally active NICD. In keeping with the hypothesized heightened transcriptional activity of the mutant NICD, Mec-1/KO^{NICD-M} clones showed the highest expression levels of both target genes (Fig. 1C-D).

These results indicate that these cell variants represent suitable models to study the role of NOTCH1 and the impact of PEST domain mutations on CLL.

RNA sequencing highlights down-modulation of genes involved in intracellular signaling and chemotaxis in Mec-1/KO cells

Two genetically distinct Mec-1/WT and Mec-1/KO clones were analyzed for gene expression by RNA sequencing. Cells were examined under standard culture conditions to highlight gene expression differences occurring at baseline. A total of 1,332 genes were differentially expressed; in KO cells, 803 genes were down-regulated and 529 up-regulated (Fig. 2A). *NOTCH1*, along with genes belonging to the gene ontology (GO) category “NOTCH1 signaling” was down-regulated in the KO cells (Fig. 2B), indirectly validating the model. In-depth analysis of the genetic pathways indicated that “intracellular signaling”, “chemotaxis”, “immune response”, and “cell proliferation” were the most frequently down-modulated on NOTCH1 loss (Fig. 2C-D). On the other hand, genes in the categories “MAPK regulation,” “response to stress,” and “apoptosis” were present in the two-fold up-modulation list (Fig. 2C-D).

Mec-1/KO cells show impaired growth and chemotaxis due to decreased MAPK signaling and STAT3 activation

In keeping with the RNAseq results, Mec-1/KO cells were characterized by diminished growth under conventional culture conditions and reduced survival upon serum deprivation. (Fig. 3A-B). Furthermore, Mec-1/KO cells showed significantly decreased chemotactic responses toward CCL19, a chemokine that drives CLL localization to the lymph nodes (21-23) (Fig. 3C). Both phenotypic behaviors were rescued by re-expression of the NICD and were further enhanced in cells expressing the NICD-M. In particular, KO^{NICD-M} clones grew more than KO^{NICD} clones, as determined by MTT assays. KO^{NICD-M} clones also showed enhanced chemotaxis towards CCL19, in keeping with the hypothesis that the PEST domain mutation confers functional advantages (Fig. 3A-C).

One possible explanation of the impaired chemotaxis of Mec-1/KO is reduced expression of *CCR7*, the CCL19 receptor, as highlighted by RNAseq data (Fig. 2D). Analysis by qRT-PCR (Fig. 3D) confirmed that *CCR7* levels were significantly lower in Mec-1/KO than in Mec-1/WT cells, as confirmed also at the protein level (fig S3A). Unlike WT cells, Mec-1/KO cells did not respond to CCL19 exposure with increased actin polymerization and cytoplasmic Ca²⁺ mobilization (fig. S3B-D). Furthermore, analysis of signal transduction indicated significantly reduced levels of MAPK tyrosine phosphorylation, both before and after the addition of CCL19. Reduced activation was evident when studying JNK, p38 and, to a lesser extent, ERK1/2, suggesting that MAPK signaling is globally disturbed in Mec-1/KO cells (Fig. 3E).

Reconstitution of these cells with NICD or NICD-M constructs restored *CCR7* expression (Fig. 3D), which was higher in the presence of the NICD-M. Reconstituted cells also exhibited restored actin polymerization (fig. S3C) and signal transduction, as indicated by tyrosine phosphorylation of JNK, p38, and, to a lesser extent, ERK1/2, both in unstimulated cells and in cells exposed to CCL19. This effect was more pronounced in $\text{KO}^{\text{NICD-M}}$ cells; specifically, the intensity (in the case of JNK phosphorylation) and duration (in the case of p38 and ERK1/2 phosphorylation) of the signal were enhanced in $\text{KO}^{\text{NICD-M}}$ cells relatively to the WT counterpart. Functionally, *Mec-1*/ KO^{NICD} cells almost completely regained the ability to migrate in response to CCL19, with *Mec-1*/ $\text{KO}^{\text{NICD-M}}$ cells exhibiting the highest migration levels (Fig. 3C).

STAT3 is a transcription factor activated by MAPKs and directly regulating *CCR7* gene expression (24). As expected from the loss of *CCR7* expression, *Mec-1*/*KO* cells showed severely compromised phosphorylation of STAT3, both before and after stimulation with CCL19, compared to the WT. This activity was restored in *Mec-1*/ KO^{NICD} and even more in *Mec-1*/ $\text{KO}^{\text{NICD-M}}$ (Fig. 3E). This observation suggests that failed STAT3-dependent gene transcription results in reduced expression of the chemokine receptor, which in turn decreases cellular chemotaxis towards CCL19.

Mec-1*/*KO* cells are characterized by an over-expression of the tumor suppressor gene *DUSP22

The RNAseq data indicated that *Mec-1*/*KO* cells expressed genes involved in negative regulation of MAPK signaling at a significantly higher levels than control cells. Seven genes were listed in this category, namely *PRKCA*, *LAX1*, *SPRED1*, *SPRED2*, *DUSP22*,

PDCD4 and *TP73* (Fig. 4A). Of these, the tumor suppressor gene *DUSP22* was the most differentially expressed between Mec-1/WT and Mec-1/KO cells (Figs. 4B and S4). Expression of this gene dropped in Mec-1/KO^{NICD} and – more significantly – in Mec-1/KO^{NICD-M} (Fig. 4B), indicating that transcriptionally active NOTCH1 impairs its expression. These differences were maintained at the protein level, as shown by WB (Fig. 4C).

DUSP22 codes for a protein phosphatase that inactivates MAPK and STAT3 (25, 26), providing a mechanistic explanation for the failed phosphorylation of STAT3 and decreased *CCR7* expression. These findings led to the working hypothesis that *DUSP22* overexpression leads to both direct and, via MAPK, indirect STAT3 inhibition, failed *CCR7* transcription, and, ultimately, decreased chemotaxis to CCL19.

To confirm this hypothesis, Mec-1/WT cells were transiently transfected with a *DUSP22*-GFP construct (Fig. 4D). Overexpression of the molecule at 24 hours was shown by WB and confirmed by flow cytometry (FC) (Fig. 4E and not shown). In line with the working hypothesis, Mec-1/WT cells overexpressing *DUSP22* were characterized by decreased STAT3 activation, *CCR7* expression, and chemotaxis toward CCL19 (Fig. 4E-F-G). Conversely, silencing of *DUSP22* expression in MEC-1/KO cells, as obtained by transfection with a specific siRNA (Fig. 4H), was followed by increased STAT3 phosphorylation, *CCR7* expression, and chemotaxis to CCL19 (Fig. 4I- K).

The NICD modulates nuclear circuits involving HDAC1 and DMT3A

To explain how *NOTCH1* and PEST domain mutations could affect *DUSP22* expression, we hypothesized a role of promoter methylation of the gene, consistent with

observations from other models (27). Therefore, a methylation-specific PCR was performed to investigate the methylation status of the *DUSP22* promoter. We found that KO clones displayed a *DUSP22* promoter that was significantly less methylated than its WT counterpart (Figs. 5A and S5A). When the NICD was reintroduced into Mec-1/KO cells, methylation of the *DUSP22* promoter increased, while gene expression decreased, suggesting a NOTCH1-dependent mechanism. Expression of the NICD-M construct showed a further and significant increase in promoter methylation (Fig. 5A). Treatment of Mec-1/WT cells with 5'-2-deoxy-azacytidine (5-AZA), which inhibits the activity of DNMT3A (28), was followed by decreased *DUSP22* promoter methylation (Fig. 5B), and subsequent significant increase in *DUSP22* mRNA levels (Fig. 5C). As expected, treated cells showed significantly decreased expression of *CCR7* (Fig. 5D), greatly impaired MAPK signaling, and STAT3 phosphorylation both before and after CCL19 stimulation (Fig. 5F) and a resultant marked decrease in CCL19-driven chemotaxis (Fig. 5E).

These findings suggest that expression of the NICD alters methylation activity of DNMT3A. Previous evidence indicates that NOTCH1 contributes to epigenetic regulation of gene expression through the displacement of HDACs from the RBPJk complex (20). Furthermore, it is known that HDAC1 can bind to and stabilize DNMT3A, thus promoting gene methylation (29, 30). Therefore, we hypothesized that the presence of the NICD, by competing with and displacing HDAC1 from its interaction with RBPJk, would promote the formation of a HDAC1/DNMT3A complex, resulting in increased methylation of the *DUSP22* promoter.

The presence of HDAC1-DNMT3A complexes was evaluated by IP assay in nuclear lysates of Mec-1/WT, Mec-1/KO, KO^{NICD} and KO^{NICD-M}. Mec-1/KO cells showed significantly lower levels of HDAC1 bound to DNMT3A, compared to the Mec-1/WT counterparts. However, the association was restored in Mec-1/KO^{NICD} and Mec-1/KO^{NICD-M} cells. In these immunoprecipitates HDAC1 was mainly found in a homodimeric form of 120 kD, which is reportedly enzymatically active (31) (Fig. 5G).

Finally, chromatin immunoprecipitation experiments confirmed that DNMT3A was bound to the *DUSP22* promoter in Mec-1/WT, KO^{NICD}, and KO^{NICD-M}, while little or no DNMT3A binding was observed in Mec-1/KO cells (Fig. 5H).

CLL patients with a *NOTCH1*-mutated clone are characterized by lower levels of *DUSP22*, increased methylation of the *DUSP22* promoter, and increased chemotaxis to CCL19

We then performed a retrospective analysis on a cohort of 113 patients with confirmed CLL diagnoses (Table S1). We first divided patients on the basis of the *NOTCH1* mutational burden, determined using a quantitative ARMS-PCR approach adapted with a SYBR-green-based method (Fig. 6A).

Using RNA samples available for 90 patients, we determined *DUSP22* mRNA levels in purified CLL cells by qRT-PCR. In agreement with previous data (32), patients showing molecular (absence of somatic mutations in the IgHV genes) or clinical (disease stage, therapy requirement) characteristics of aggressive disease displayed significantly lower *DUSP22* levels (fig. S6A-C). Furthermore, in this cohort, *DUSP22* expression was inversely correlated to the percentage of *NOTCH1*-mutated alleles (Fig. 6B). By applying a

previously defined cut-off for variant allele frequency (VAF) of 12% (33), patients were divided into two groups, with those <12% considered subclonal. According to this classification, 56 patients harbored clonal *NOTCH1* mutations, while the remaining 34 patients were in the subclonal range. Significantly lower *DUSP22* levels characterized patients with a clonal *NOTCH1* mutation as compared to patients with subclonal mutations (Fig. 6C). This finding was confirmed at the protein level in a small subgroup of patients, by determining *DUSP22* expression in whole cell lysates (Fig. 6F). By monitoring *DUSP22* mRNA levels in sequential samples collected from five patients, we observed a decrease in expression as the *NOTCH1*-mutated clone expanded and vice-versa (Figs. 6D and S6D).

In concordance with observations of the cell line model, differences in *DUSP22* expression were due to different levels of methylation of the *DUSP22* promoter: clinical samples showing low levels of *DUSP22* mRNA were characterized by higher methylation of the promoter (Fig. 6E). In addition, patients with low *DUSP22* mRNA levels were characterized by a more marked constitutive STAT3 phosphorylation (Fig. 6F), higher *CCR7* mRNA expression levels (Fig. 6G), and, ultimately, enhanced chemotaxis towards CCL19 (Fig. 6H).

Generation of a Mec-1 variant carrying truncating mutations on NOTCH1 PEST domain

The data obtained indicate that NOTCH1 signaling regulates nuclear circuits, which in turn affect the expression of genes involved in growth and in chemotaxis towards CCL19. This suggests that the cells' ability to reach peripheral lymphoid organs, where

the antigen and co-stimulatory signals are available, may differ according to *NOTCH1* mutational status.

To study the impact of *NOTCH1* PEST domain mutations *in vivo*, we again exploited CRISPR/Cas9 technology to generate a Mec-1 variant with PEST domain mutations (fig. S1A). To this end, Mec-1 cells were transiently transfected with a Cas9-GFP construct and an RNA guide driving the enzyme to cut *NOTCH1* exon 34 in position 7478 (Reference sequence: NM_017617.3). GFP⁺ cells were sorted, cloned by serial dilutions, and analyzed by Sanger sequencing to identify missense mutations originated by the NHEJ-mediated DNA repair. The mutations truncate *NOTCH1* PEST domain, mirroring the Δ CT_7541-7542 mutation that has been described in CLL patients and is carried by Mec-1/KO^{NICD-M} cells. Three clones with different frameshift insertion/deletions up to 8 nucleotides (indicated as Mec-1/PEST, P2493*fs) were established (fig. S7A). Similar to primary CLL cells, these clones were heterozygous, expressing both the WT and the mutant alleles, as documented by WB (fig. S7B).

As expected, under steady-state conditions *in vitro* these cells did not show significant differences from WT cells in terms of constitutive NOTCH1 pathway activation (fig. S7D-E). They consistently required engagement by the ligand to initiate signaling (15). This conclusion was reached after the NICD band appeared upon co-culture of Mec-1/WT or Mec-1/PEST cells with human bone marrow stromal cells (HS-5) that had been transduced with a lentiviral vector to overexpress either *Jagged1* or *DLL1* (Figs. 7A and S8). In these conditions, the NICD-PEST was more stable than the NICD-WT, as shown by monitoring protein stability following leukemia-stroma co-cultures. Results indicate that

the NICD-WT disappeared rapidly once leukemic cells were separated from the ligand-expressing stroma, as predicted in physiological conditions. In contrast, the NICD-PEST remained visible by WB up to 24 hours after ending the co-cultures (Fig. 7B-C). In line with this observation, expression of the NOTCH1 target gene *HES1* in Mec-1/PEST cells was significantly higher than in Mec-1/WT cells up to eight hours after ending the co-culture (Fig. 7D). Interestingly, activation of NOTCH1 signaling induced by HS-5 correlated with a significant decrease of *DUSP22* expression, compared to cells cultured alone (Fig. 7E). The effect was more pronounced in Mec-1/PEST cells (Fig. 7E), in which *DUSP22* levels remained significantly down-modulated up to 24 hours after ending the co-culture (fig. S7F). In line with the working hypothesis, *CCR7* levels were increased upon co-culture on HS-5, with the strongest effect in the PEST clones (Fig. 7F).

These results suggest that Mec-1/PEST cells, while less serviceable for functional studies *in vitro*, can be effectively exploited in xenograft models, due to the documented cross-reactivity between human and mouse NOTCH1 ligands (34). When tested, a prominent band corresponding to the WT or mutant NICD was in fact observed after recovering Mec-1/WT or /PEST from immunocompromised mice (fig. S7G).

Mec-1/WT, Mec-1/KO and Mec-1/PEST show different spreading in xenograft models

We compared engraftment and spreading of Mec-1/WT, /KO, and /PEST clones in NOD/SCID/ γ -chain^{-/-} (NSG) mice. Mice were injected intravenously (i.v.) with at least two different clones for each of the Mec-1 lines. Subsequent engraftment was monitored by magnetic resonance imaging (MRI) performed two and three weeks post-injection. While all cell lines showed 100% engraftment, colonization was markedly different.

Mec-1/KO cells localized to the kidney but showed limited diffusion to other parenchymatous and non-parenchymatous organs in the following weeks (Fig. 8A). In contrast, mice xenografted with Mec-1/WT cells showed both renal disease and nodal metastases to the liver (Fig. 8A). Microscopically, FC analysis for CD19 and CD20 approximately four weeks after engraftment also demonstrated human leukemic cells in the spleen and in the brain. Animals engrafted with Mec-1/PEST cells were characterized by the least kidney involvement (Fig. 8A-C), by liver disease comparable to the Mec-1/WT mice (fig. S9A-B), and by markedly greater involvement of the spleen and the brain. This was documented both macroscopically, as the spleens obtained by Mec-1/PEST were significantly heavier than those of the two other animal groups (Fig. 8B), and microscopically, by leukemic cell count or immunohistochemical analysis (Fig. 8C-G). In accordance with *in vitro* results, *DUSP22* mRNA levels were markedly decreased both in Mec-1/WT and/PEST cells recovered after *in vivo* growth (fig. S9D). These results suggest that Mec-1/PEST cells have a unique tropism towards the spleen and brain, two organs in which an active role for CCL19 has been identified (35, 36).

Discussion

After the systematic application of next-generation sequencing technologies to the analysis of cancer cells, scientists have assembled an incredible wealth of novel data on the genomic architecture of tumors. However, the functional role of these mutations in the development and progression of diseases such as CLL remain to be fully elucidated(37). *NOTCH1* mutations were among the first to be identified using whole exome sequencing, and their prevalence and prognostic power for CLL patients has since been extensively studied (6). To address the question of the role of NOTCH1 in CLL biology and identify the effects of its most commonly represented mutation, we exploited the CRISPR/Cas9 technology to re-create *NOTCH1* mutations typical of CLL patients in a cell line model. Based on patient analysis, computer predictions, and previous studies (16), these mutations would appear to have a milder phenotypic impact, far from the strong and driving effect of NOTCH1 mutations in acute leukemia.

The first approach was to compare the transcriptome of cells expressing a WT NOTCH1 to that of cells lacking the gene, to highlight the NOTCH1-regulated pathways. We then reconstituted Mec-1/KO cells with a WT or M NICD and studied their behavior. Using this approach, growth and chemotaxis were the two pathways most impacted by NOTCH1 loss. Consistently, Mec-1/KO cells grew less rapidly and migrated less towards CCL19 than their WT or reconstituted counterparts. Importantly, in all biologic assays clones reconstituted with a NICD-M construct performed slightly but significantly better than clones reconstituted with a NICD-WT, in line with the predicted mild effect of the mutation. The model that we propose to explain these observations is based on a

nuclear ecosystem composed of four molecular actors: NICD, RBPJk, HDAC1, and DNMT3A. These four molecules interact as follows: NICD needs RBPJk to form a functional transcriptional complex; however, in the absence of NICD, RBPJk is bound to HDAC1 in a repressor complex. In turn, HDAC1 can bind and stabilize DNMT3A, promoting its activity (fig. S10). It is a reasonable presumption that even a slight modification in the stability of the NICD can perturb these interactions, ultimately modulating DNMT3A activity.

In the CLL model analyzed, *DUSP22* is a key target molecule of DNMT3A activity. Hence, bioavailability of the NICD directly affects methylation levels in the *DUSP22* promoter, ultimately regulating its expression. Confirmation of this hypothesis was obtained by showing that the *DUSP22* promoter was hypomethylated in Mec-1/KO and hypermethylated in KO^{NICD} and KO^{NICD-M} cells. Expression of the molecule were consistently highest in Mec-1/KO cells and lowest in KO^{NICD-M} cells.

DUSP22 is a member of the dual-specific phosphatase family. It modulates activity of MAPK family members, including JNK (both activated and inactivated) and p38 (inactivated), and it inactivates STAT3 (25, 26, 38). Recent studies in colon cancer cells have revealed that this molecule may act as a tumor suppressor, as its loss is associated with increased migration and motility, as well as an inferior outcome (39). In CLL cells, *DUSP22* is overexpressed, correlating with the presence of somatic mutation in the IgHV genes (32), in the subset of patients with good prognosis.

As expected with an increased expression of DUSP22, Mec-1/KO showed constitutively decreased STAT3 phosphorylation, which in turn is a transcriptional regulator of *CCR7*,

the CCL19 receptor. Consequently, Mec-1/KO clones showed the lowest *CCR7* expression and the lowest chemotactic responses to CCL19. On the contrary, Mec-1/KO^{NICD-M} showed the highest levels of baseline STAT3 phosphorylation, with the highest levels of *CCR7* expression and subsequent CCL19-driven chemotaxis. Silencing of *DUSP22* in Mec-1/KO and overexpression in Mec-1/WT confirmed that STAT3 phosphorylation, *CCR7* expression, and chemotaxis are directly impacted by modulation of *DUSP22* levels.

These observations were confirmed in a large cohort of primary cases. By comparing primary CLL cells carrying *NOTCH1* mutations at the clonal and subclonal levels, we observed significantly hypermethylation of *DUSP22* with lower mRNA and protein levels in clonal compared with subclonal patients. The clonal subset consistently showed constitutive STAT3 phosphorylation, expressed higher levels of *CCR7*, and migrated more efficiently to CCL19 than the subclonal subset.

We then used CRISPR/Cas9 technology to generate cells with a mutation pattern similar to that observed in patients. Several clones with a shorter PEST domain were generated and studied. Our study shows that cells carrying a WT or a PEST domain mutant *NOTCH1* must still interact with the ligand to activate *NOTCH1* pathway. By following the signaling pathway over time, we confirmed that, at the molecular level, PEST domain mutations increase the stability of the NICD and maintain the activation of *NOTCH1* signaling for longer, when compared to the WT. Moreover, ligand-mediated *NOTCH1* activation resulted in a further decrease of *DUSP22* levels, confirming *NOTCH1*-dependent modulation.

Even if this model has intrinsic limitations for *in vitro* studies, it may be used *in vivo*, where mouse Jagged and DLL family molecules are reported to bind and activate human NOTCH1 (16, 34). Xenograft studies showed that Mec-1/PEST clones were characterized by markedly increased metastatic properties, with extensive colonization of the liver, the spleen, and the brain, in contrast to the Mec-1/KO cells, which remained predominantly localized in the kidney, the first engrafted organ (40).

Intriguingly, CCR7 has been previously recognized as an entry signal to the brain for leukemic cells, and activating mutations of NOTCH1 have been found to increase *CCR7* expression (35). CLL localization to the brain is infrequent; however, there are reports of central nervous system infiltration occurring with RS. As *NOTCH1* mutations have been proposed as a risk factor for RS, future studies are needed to understand if this patient subset may have a higher risk of CNS localization of the disease.

Considered together, these results show that PEST domain mutations increase the stability of the NICD and the expression of NOTCH1 target genes, in turn affecting a complex nuclear balance. The final outcome for the CLL cell is decreased expression of the tumor suppressor gene *DUSP22*, with modification in the migratory properties of the leukemic cell. As CCL19 regulates homing to secondary organs, one could speculate that *NOTCH1* mutations may favor CLL recirculation to lymph nodes and spleen, where the local environment favors proliferation and protection from apoptosis, two conditions that are associated with a more aggressive disease process and an unfavorable prognosis.

Experimental procedures

Study design

The aim of the study was to highlight NOTCH1-dependent mechanisms contributing to CLL pathogenesis and progression, as well as the advantages that PEST domain truncating mutations confer to leukemic cells. Mec-1, an accepted NOTCH1-WT CLL-like model was exploited to generate a working model, overcoming the intrinsic limits of primary CLL cells that have so far restrained a mechanistic characterization of NOTCH1 functional role. Two parallel but integrated strategies were adopted, both based on the CRISPR/Cas9 system. First, we generated a *NOTCH1*-KO Mec-1 model to identify NOTCH1-regulated cellular processes, by comparing the transcriptome profile of the KO and WT cells. Expression of the NICD-WT or NICD-PEST was restored in KO cells by lentiviral infection. These models were used to rescue the KO phenotype and to study the behavior of the mutant. The findings were then confirmed on samples from CLL patients, obtained after informed consent, in accordance with Institutional Guidelines and the Declaration of Helsinki.

Second, we directed Cas9 on exon34 of NOTCH1 to truncate the PEST domain, recreating the mutation seen in CLL patients. This second approach was pursued to characterize the behavior of PEST-mutated cells *in vivo* where leukemic cells are known to find the ligand, which is necessary to generate the NICD and to activate signaling. *In vivo* studies were performed according to Institutional Guidelines and with the approval of the Animal Care Committee of the University of Turin and the Italian Ministry of Health.

Experimental Methods

Detailed descriptions of experimental methods are provided in Supplementary Materials and Methods.

Statistical Analyses

Statistical analyses were performed with GraphPad v6 (GraphPad Software Inc, La Jolla, CA, USA) and are presented as box plots or scatter plots. In the text, data are presented as mean \pm SD. Mann-Whitney or Wilcoxon matched-pairs signed rank test were used to determine statistical significance. In the case of grouped analyses (time- and variant-dependent results), statistics were performed with the 2-way ANOVA test. $P < 0.05$ (*); $P < 0.01$ (**); $P < 0.001$ (***); $P > 0.0001$ (****).

Supplementary Materials

Materials and Methods

Fig. S1. Schematic view of the working model generated by CRISPR/Cas9.

Fig. S2. IP of NOTCH1 in Mec-1/KO, KO^{NICD} and KO^{NICD-M}.

Fig. S3. Calcium fluxes and Actin polymerization in response to CCL19

Fig. S4. qRT-PCR of other genes encoding negative regulators of MAPK.

Fig. S5. Example of MS-PCR image and control experiments validating the nuclear complex

Fig. S6. Analysis of *DUSP22* levels in CLL samples divided according to clinical and molecular features

Fig. S7. Validation of Mec-1/PEST cells

Fig. S8. FC analysis of ligand expression in HS-5 cells

Fig. S9. Liver engraftment of Mec-1 variant and additional IHC images

References

1. N. Villamor, L. Conde, A. Martinez-Trillos, M. Cazorla, A. Navarro, S. Bea, C. Lopez, D. Colomer, M. Pinyol, M. Aymerich, M. Rozman, P. Abrisqueta, T. Baumann, J. Delgado, E. Gine, M. Gonzalez-Diaz, J. M. Hernandez, E. Colado, A. R. Payer, C. Rayon, B. Navarro, M. Jose Terol, F. Bosch, V. Quesada, X. S. Puente, C. Lopez-Otin, P. Jares, A. Pereira, E. Campo, A. Lopez-Guillermo, NOTCH1 mutations identify a genetic subgroup of chronic lymphocytic leukemia patients with high risk of transformation and poor outcome. *Leukemia* **27**, 1100-1106 (2013).
2. X. S. Puente, M. Pinyol, V. Quesada, L. Conde, G. R. Ordóñez, N. Villamor, G. Escaramis, P. Jares, S. Bea, M. Gonzalez-Diaz, L. Bassaganyas, T. Baumann, M. Juan, M. Lopez-Guerra, D. Colomer, J. M. Tubio, C. Lopez, A. Navarro, C. Tornador, M. Aymerich, M. Rozman, J. M. Hernandez, D. A. Puente, J. M. Freije, G. Velasco, A. Gutierrez-Fernandez, D. Costa, A. Carrio, S. Guijarro, A. Enjuanes, L. Hernandez, J. Yague, P. Nicolas, C. M. Romeo-Casabona, H. Himmelbauer, E. Castillo, J. C. Dohm, S. de Sanjose, M. A. Piris, E. de Alava, J. San Miguel, R. Royo, J. L. Gelpi, D. Torrents, M. Orozco, D. G. Pisano, A. Valencia, R. Guigo, M. Bayes, S. Heath, M. Gut, P. Klatt, J. Marshall, K. Raine, L. A. Stebbings, P. A. Futreal, M. R. Stratton, P. J. Campbell, I. Gut, A. Lopez-Guillermo, X. Estivill, E. Montserrat, C. Lopez-Otin, E. Campo, Whole-genome sequencing identifies recurrent mutations in chronic lymphocytic leukaemia. *Nature* **475**, 101-105 (2011).

3. G. Fabbri, H. Khiabani, A. B. Holmes, J. Wang, M. Messina, C. G. Mullighan, L. Pasqualucci, R. Rabadan, R. Dalla-Favera, Genetic lesions associated with chronic lymphocytic leukemia transformation to Richter syndrome. *J Exp Med* **210**, 2273-2288 (2013).
4. D. A. Landau, E. Tausch, A. N. Taylor-Weiner, C. Stewart, J. G. Reiter, J. Bahlo, S. Kluth, I. Bozic, M. Lawrence, S. Bottcher, S. L. Carter, K. Cibulskis, D. Mertens, C. L. Sougnez, M. Rosenberg, J. M. Hess, J. Edelman, S. Kless, M. Kneba, M. Ritgen, A. Fink, K. Fischer, S. Gabriel, E. S. Lander, M. A. Nowak, H. Dohner, M. Hallek, D. Neuberg, G. Getz, S. Stilgenbauer, C. J. Wu, Mutations driving CLL and their evolution in progression and relapse. *Nature* **526**, 525-530 (2015).
5. D. Rossi, S. Rasi, V. Spina, A. Bruscaggin, S. Monti, C. Ciardullo, C. Deambrogi, H. Khiabani, R. Serra, F. Bertoni, F. Forconi, L. Laurenti, R. Marasca, M. Dal-Bo, F. M. Rossi, P. Bulian, J. Nomdedeu, G. Del Poeta, V. Gattei, L. Pasqualucci, R. Rabadan, R. Foa, R. Dalla-Favera, G. Gaidano, Integrated mutational and cytogenetic analysis identifies new prognostic subgroups in chronic lymphocytic leukemia. *Blood* **121**, 1403-1412 (2013).
6. G. Fabbri, S. Rasi, D. Rossi, V. Trifonov, H. Khiabani, J. Ma, A. Grunn, M. Fangazio, D. Capello, S. Monti, S. Cresta, E. Gargiulo, F. Forconi, A. Guarini, L. Arcaini, M. Paulli, L. Laurenti, L. M. Larocca, R. Marasca, V. Gattei, D. Oscier, F. Bertoni, C. G. Mullighan, R. Foa, L. Pasqualucci, R. Rabadan, R. Dalla-Favera, G. Gaidano, Analysis of the chronic lymphocytic leukemia coding genome: role of NOTCH1 mutational activation. *J Exp Med* **208**, 1389-1401 (2011).

7. I. Del Giudice, D. Rossi, S. Chiaretti, M. Marinelli, S. Tavoraro, S. Gabrielli, L. Laurenti, R. Marasca, S. Rasi, M. Fangazio, A. Guarini, G. Gaidano, R. Foa, NOTCH1 mutations in +12 chronic lymphocytic leukemia (CLL) confer an unfavorable prognosis, induce a distinctive transcriptional profiling and refine the intermediate prognosis of +12 CLL. *Haematologica* **97**, 437-441 (2012).
8. S. Weissmann, A. Roller, S. Jeromin, M. Hernandez, M. Abaigar, J. M. Hernandez-Rivas, V. Grossmann, C. Haferlach, W. Kern, T. Haferlach, S. Schnittger, A. Kohlmann, Prognostic impact and landscape of NOTCH1 mutations in chronic lymphocytic leukemia (CLL): a study on 852 patients. *Leukemia* **27**, 2393-2396 (2013).
9. P. Baliakas, A. Hadzidimitriou, L. A. Sutton, D. Rossi, E. Minga, N. Villamor, M. Larrayoz, J. Kminkova, A. Agathangelidis, Z. Davis, E. Tausch, E. Stalika, B. Kantorova, L. Mansouri, L. Scarfo, D. Cortese, V. Navrkalova, M. J. Rose-Zerilli, K. E. Smedby, G. Juliusson, A. Anagnostopoulos, A. M. Makris, A. Navarro, J. Delgado, D. Oscier, C. Belessi, S. Stilgenbauer, P. Ghia, S. Pospisilova, G. Gaidano, E. Campo, J. C. Strefford, K. Stamatopoulos, R. Rosenquist, Recurrent mutations refine prognosis in chronic lymphocytic leukemia. *Leukemia* **29**, 329-336 (2015).
10. D. Rossi, G. Gaidano, Richter syndrome: pathogenesis and management. *Seminars in oncology* **43**, 311-319 (2016).
11. L. A. Sutton, R. Rosenquist, Deciphering the molecular landscape in chronic lymphocytic leukemia: time frame of disease evolution. *Haematologica* **100**, 7-16 (2015).

12. F. Morabito, L. Mosca, G. Cutrona, L. Agnelli, G. Tuana, M. Ferracin, B. Zagatti, M. Lionetti, S. Fabris, F. Maura, S. Matis, M. Gentile, E. Vigna, M. Colombo, C. Massucco, A. G. Recchia, S. Bossio, L. De Stefano, F. Ilariucci, C. Musolino, S. Molica, F. Di Raimondo, A. Cortelezzi, P. Tassone, M. Negrini, S. Monti, D. Rossi, G. Gaidano, M. Ferrarini, A. Neri, Clinical monoclonal B lymphocytosis versus Rai 0 chronic lymphocytic leukemia: A comparison of cellular, cytogenetic, molecular, and clinical features. *Clinical cancer research : an official journal of the American Association for Cancer Research* **19**, 5890-5900 (2013).
13. J. Ojha, C. Secreto, K. Rabe, J. Ayres-Silva, R. Tschumper, D. V. Dyke, S. Slager, R. Fonseca, T. Shanafelt, N. Kay, E. Braggio, Monoclonal B-cell lymphocytosis is characterized by mutations in CLL putative driver genes and clonal heterogeneity many years before disease progression. *Leukemia* **28**, 2395-2398 (2014).
14. D. A. Landau, C. J. Wu, Chronic lymphocytic leukemia: molecular heterogeneity revealed by high-throughput genomics. *Genome Med* **5**, 47 (2013).
15. F. Arruga, B. Gizdic, S. Serra, T. Vaisitti, C. Ciardullo, M. Coscia, L. Laurenti, G. D'Arena, O. Jaksic, G. Inghirami, D. Rossi, G. Gaidano, S. Deaglio, Functional impact of NOTCH1 mutations in chronic lymphocytic leukemia. *Leukemia* **28**, 1060-1070 (2014).
16. E. Rosati, R. Sabatini, G. Rampino, A. Tabilio, M. Di Ianni, K. Fettucciari, A. Bartoli, S. Coaccioli, I. Screpanti, P. Marconi, Constitutively activated Notch signaling is involved in survival and apoptosis resistance of B-CLL cells. *Blood* **113**, 856-865 (2009).

17. P. Secchiero, E. Melloni, M. G. di Iasio, M. Tiribelli, E. Rimondi, F. Corallini, V. Gattei, G. Zauli, Nutlin-3 up-regulates the expression of Notch1 in both myeloid and lymphoid leukemic cells, as part of a negative feedback antiapoptotic mechanism. *Blood* **113**, 4300-4308 (2009).
18. P. Ntziachristos, J. S. Lim, J. Sage, I. Aifantis, From Fly Wings to Targeted Cancer Therapies: A Centennial for Notch Signaling. *Cancer cell* **25**, 318-334 (2014).
19. K. G. Guruharsha, M. W. Kankel, S. Artavanis-Tsakonas, The Notch signalling system: recent insights into the complexity of a conserved pathway. *Nat Rev Genet* **13**, 654-666 (2012).
20. F. Pozzo, T. Bittolo, F. Arruga, P. Bulian, P. Macor, E. Tissino, B. Gizdic, F. M. Rossi, R. Bomben, A. Zucchetto, D. Benedetti, M. Degan, G. D'Arena, A. Chiarenza, F. Zaja, G. Pozzato, D. Rossi, G. Gaidano, G. Del Poeta, S. Deaglio, V. Gattei, M. Dal Bo, NOTCH1 mutations associate with low CD20 level in chronic lymphocytic leukemia: evidence for a NOTCH1 mutation-driven epigenetic dysregulation. *Leukemia* **30**, 182-189 (2016).
21. G. Malet-Engra, J. Viaud, L. Ysebaert, M. Farce, F. Lafouresse, G. Laurent, F. Gaits-Iacovoni, G. Scita, L. Dupre, CIP4 controls CCL19-driven cell steering and chemotaxis in chronic lymphocytic leukemia. *Cancer research* **73**, 3412-3424 (2013).
22. C. Cuesta-Mateos, S. Lopez-Giral, M. Alfonso-Perez, V. G. de Soria, J. Loscertales, S. Guasch-Vidal, A. E. Beltran, J. M. Zapata, C. Munoz-Calleja, Analysis of migratory and prosurvival pathways induced by the homeostatic chemokines

- CCL19 and CCL21 in B-cell chronic lymphocytic leukemia. *Experimental hematology* **38**, 756-764, 764 e751-754 (2010).
23. R. Forster, A. Schubel, D. Breitfeld, E. Kremmer, I. Renner-Muller, E. Wolf, M. Lipp, CCR7 coordinates the primary immune response by establishing functional microenvironments in secondary lymphoid organs. *Cell* **99**, 23-33 (1999).
 24. K. Jiang, L. C. Krous, N. Knowlton, Y. Chen, M. B. Frank, C. Cadwell, M. Centola, J. N. Jarvis, Ablation of Stat3 by siRNA alters gene expression profiles in JEG-3 cells: a systems biology approach. *Placenta* **30**, 806-815 (2009).
 25. Y. Sekine, O. Ikeda, Y. Hayakawa, S. Tsuji, S. Imoto, N. Aoki, K. Sugiyama, T. Matsuda, DUSP22/LMW-DSP2 regulates estrogen receptor-alpha-mediated signaling through dephosphorylation of Ser-118. *Oncogene* **26**, 6038-6049 (2007).
 26. Y. Sekine, S. Tsuji, O. Ikeda, N. Sato, N. Aoki, K. Aoyama, K. Sugiyama, T. Matsuda, Regulation of STAT3-mediated signaling by LMW-DSP2. *Oncogene* **25**, 5801-5806 (2006).
 27. J. V. Sanchez-Mut, E. Aso, H. Heyn, T. Matsuda, C. Bock, I. Ferrer, M. Esteller, Promoter hypermethylation of the phosphatase DUSP22 mediates PKA-dependent TAU phosphorylation and CREB activation in Alzheimer's disease. *Hippocampus* **24**, 363-368 (2014).
 28. M. Oka, A. M. Meacham, T. Hamazaki, N. Rodic, L. J. Chang, N. Terada, De novo DNA methyltransferases Dnmt3a and Dnmt3b primarily mediate the cytotoxic effect of 5-aza-2'-deoxycytidine. *Oncogene* **24**, 3091-3099 (2005).

29. L. Yang, R. Rau, M. A. Goodell, DNMT3A in haematological malignancies. *Nature reviews. Cancer* **15**, 152-165 (2015).
30. D. Liu, P. Zhou, L. Zhang, W. Gong, G. Huang, Y. Zheng, F. He, HDAC1/DNMT3A-containing complex is associated with suppression of Oct4 in cervical cancer cells. *Biochemistry (Mosc)* **77**, 934-940 (2012).
31. D. H. Khan, S. He, J. Yu, S. Winter, W. Cao, C. Seiser, J. R. Davie, Protein kinase CK2 regulates the dimerization of histone deacetylase 1 (HDAC1) and HDAC2 during mitosis. *The Journal of biological chemistry* **288**, 16518-16528 (2013).
32. E. Jantus Lewintre, C. Reinoso Martin, D. Montaner, M. Marin, M. Jose Terol, R. Farras, I. Benet, J. J. Calvete, J. Dopazo, J. Garcia-Conde, Analysis of chronic lymphocytic leukemia transcriptomic profile: differences between molecular subgroups. *Leukemia & lymphoma* **50**, 68-79 (2009).
33. F. Nadeu, J. Delgado, C. Royo, T. Baumann, T. Stankovic, M. Pinyol, P. Jares, A. Navarro, D. Martin-Garcia, S. Bea, I. Salaverria, C. Oldreive, M. Aymerich, H. Suarez-Cisneros, M. Rozman, N. Villamor, D. Colomer, A. Lopez-Guillermo, M. Gonzalez, M. Alcoceba, M. J. Terol, E. Colado, X. S. Puente, C. Lopez-Otin, A. Enjuanes, E. Campo, Clinical impact of clonal and subclonal TP53, SF3B1, BIRC3, NOTCH1, and ATM mutations in chronic lymphocytic leukemia. *Blood* **127**, 2122-2130 (2016).
34. T. M. Schmitt, J. C. Zuniga-Pflucker, Induction of T cell development from hematopoietic progenitor cells by delta-like-1 in vitro. *Immunity* **17**, 749-756 (2002).

35. S. Buonomi, T. Trimarchi, M. G. Ruocco, L. Reavie, S. Cathelin, B. G. Mar, A. Klinakis, Y. Lukyanov, J. C. Tseng, F. Sen, E. Gehrie, M. Li, E. Newcomb, J. Zavadil, D. Meruelo, M. Lipp, S. Ibrahim, A. Efstratiadis, D. Zagzag, J. S. Bromberg, M. L. Dustin, I. Aifantis, CCR7 signalling as an essential regulator of CNS infiltration in T-cell leukaemia. *Nature* **459**, 1000-1004 (2009).
36. Y. W. Jung, H. G. Kim, C. J. Perry, S. M. Kaech, CCR7 expression alters memory CD8 T-cell homeostasis by regulating occupancy in IL-7- and IL-15-dependent niches. *Proceedings of the National Academy of Sciences of the United States of America* **113**, 8278-8283 (2016).
37. L. A. Sutton, R. Rosenquist, The complex interplay between cell-intrinsic and cell-extrinsic factors driving the evolution of chronic lymphocytic leukemia. *Seminars in cancer biology* **34**, 22-35 (2015).
38. J. P. Li, Y. N. Fu, Y. R. Chen, T. H. Tan, JNK pathway-associated phosphatase dephosphorylates focal adhesion kinase and suppresses cell migration. *The Journal of biological chemistry* **285**, 5472-5478 (2010).
39. D. Yu, Z. Li, M. Gan, H. Zhang, X. Yin, S. Tang, L. Wan, Y. Tian, S. Zhang, Y. Zhu, M. Lai, D. Zhang, Decreased expression of dual specificity phosphatase 22 in colorectal cancer and its potential prognostic relevance for stage IV CRC patients. *Tumour biology : the journal of the International Society for Oncodevelopmental Biology and Medicine* **36**, 8531-8535 (2015).
40. T. Vaisitti, V. Audrito, S. Serra, R. Buonincontri, G. Sociali, E. Mannino, A. Pagnani, A. Zucchetto, E. Tissino, C. Vitale, M. Coscia, C. Usai, C. Pepper, V. Gattei, S.

Bruzzone, S. Deaglio, The enzymatic activities of CD38 enhance CLL growth and trafficking: implications for therapeutic targeting. *Leukemia* **29**, 356-368 (2015).

Acknowledgements: Supported by the Associazione Italiana per la Ricerca sul Cancro AIRC (IG-17314 to SD, IG-15217 to SO and 5x1000 #100007 to GG), by the Human Genetics Foundation Institutional funds, by the Italian Ministries of Education, University and Research (Futuro in Ricerca 2012 # RBFR12D1CB), the Italian Ministry of Health (Bando Giovani Ricercatori GR-2011-02346826 and Bando Ricerca Finalizzata RF-2011-02349712), the Fondazione Cariplo, grant #2012-0689 and local university funds (ex-60%).

Author contributions: FA: designed the study, performed experiments, analyzed and interpreted data and together with SD wrote the paper; BG, CB, SC, RB, SS, TV, KG, NV, GGar, EM, SR, FN performed experiments; MC, JA, RRF, DR, GGai: provided patient samples and relevant clinical information and contributed to data interpretation; RP and SO: discussed results and contributed to data interpretation; SD: designed the study, interpreted data and together with FA wrote the paper.

Competing interests: There is no conflict of interest to declare.

Figure Legends

Fig. 1. Generation of a cell line model based on Mec-1 CLL-like cells. (A) WB analysis of NOTCH1 expression in the Mec-1 variants. Lane #1 and 2: Mec-1/WT; Lane #3 and 4: Mec-1/KO; Lane #5 and 6: Mec-1/KO^{NICD}; Lane #7 and 8: Mec-1/KO^{NICD-M}. Actin was used as loading control. **(B)** qRT-PCR analysis of *NOTCH1* levels in Mec-1 variants. qRT-PCR analysis of *HES1* **(C)** and *DTX1* **(D)** expression in Mec-1 variants.

Fig. 2. Mec-1/WT and /KO cells differentially express genes involved in the regulation of proliferation and chemotaxis. (A) Venn diagram summarizing the differentially expressed genes in Mec-1/WT and KO cells. **(B)** Heatmap of the “NOTCH1 signaling” GO. **(C)** Cumulative graph showing the GO clusters more significantly (Log10 p-value) up- or down-modulated in the Mec-1/WT and KO cells. **(D)** Heatmaps and gene lists of the differentially modulated GO clusters “chemotaxis”, “proliferation”, “MAPK regulation” and “apoptosis”. Two independent clones were analyzed, indicated by #1 and #2.

Fig. 3. NOTCH1 expression impacts on the proliferation and the migratory potential of leukemic cells. (A) Absorbance values of MTT assays (arbitrary units, a.u.). Values are represented on a log2 scale. **(B)** Viability curve of Mec-1 variants cultured for the indicated time points under stressed culture condition (RPMI 1%FCS). Apoptosis was measured and the percentage of Annexin V⁺/PI⁺ population was monitored and plotted. Statistically significant differences at 72h were: WT vs. KO $P=0.0001$; KO vs. KO^{NICD} $P=0.001$; KO vs. KO^{NICD-M} $P=0.001$. **(C)** Chemotaxis vs. CCL19. Dashed line indicates spontaneous cell migration in the absence of CCL19. **(D)** qRT-PCR analysis of *CCR7* levels in Mec-1 variants. Values are represented in a log2 scale. **(E)** WB analysis of MAPK

activation in response to CCL19 stimulation. Phosphorylation on JNK, p38, ERK1/2, and STAT3 was evaluated in the different Mec-1 variants at basal conditions (-) and after stimulation with CCL19 (+) for the indicated time points. Levels of non-phosphorylated JNK, p38, ERK1/2, and STAT3 are shown as controls.

Fig. 4. Expression of *DUSP22* modulates the chemotactic response to CCL19. (A) Heatmap of the genes annotated in the GO “Negative regulators of MAPK” showing increased expression in the KO cells. **(B)** qRT-PCR analysis of *DUSP22* expression in Mec-1 variants. Values are represented on a linear scale. **(C)** WB analysis of *DUSP22* (indicated by the arrow) in Mec-1 variants. **(D)** qRT-PCR analysis of *DUSP22* levels in transiently transfected Mec-1/WT. **(E)** WB analysis of *DUSP22* expression (TR, transfected; E, endogenous) and STAT3 phosphorylation in Mec-1/ WT cells transiently transfected with GFP alone or with a *DUSP22*-GFP plasmid. Transfected *DUSP22* is found at a different molecular weight from the endogenous one because of a GFP-tag. Levels of non-phosphorylated STAT3 are shown as control. **(F)** qRT-PCR analysis of *CCR7* expression in transiently transfected Mec-1/WT. **(G)** Chemotaxis vs. CCL19, in GFP- and *DUSP22*- transfected Mec-1/WT. **(H)** qRT-PCR analysis of *DUSP22* levels in Mec-1/KO cells transiently transfected with a scrambled (Scr) siRNA or a *DUSP22*-targeting siRNA. **(I)** WB analysis of *DUSP22* expression and STAT3 phosphorylation in Mec-1/ KO cells transiently transfected with Scr siRNA or with a *DUSP22*-siRNA. Levels of non-phosphorylated STAT3 are shown as controls. **(J)** qRT-PCR analysis of *CCR7* expression in transiently transfected Mec-1/KO. **(K)** Chemotaxis vs. CCL19 in Scr- and siRNA *DUSP22*-transfected Mec-1/KO.

Fig. 5. Differential expression of DUSP22 is due to a different methylation pattern as a consequence of NICD-modulated nuclear complexes. (A) MS-PCR of Mec-1 variants. Results are represented in a log2 scale. **(B)** MS-PCR of Mec-1/WT treated with 5-AZA or DMSO. **(C)** qRT-PCR analysis of *DUSP22* levels in Mec-1/WT treated with 5-AZA or DMSO. Values are represented on a log2 scale. **(D)** qRT-PCR analysis of *CCR7* expression in Mec-1/WT treated with 5-AZA or DMSO. **(E)** Chemotaxis vs. CCL19 in Mec-1/WT treated with 10 μ M 5-AZA or DMSO. Results are represented on a log2 scale. **(F)** WB analysis of MAPK activation in response to CCL19 stimulation in Mec-1/WT treated with 5-AZA or DMSO. Phosphorylation on JNK, p38, ERK1/2, and STAT3 was evaluated at basal conditions (-) and after stimulation with CCL19 (+) for the indicated time points. Levels of non-phosphorylated JNK, p38, ERK1/2, and STAT3 are shown as control. **(G)** Identification of a nuclear complex containing HDAC1 and DNMT3A. DNMT3A was immunoprecipitated in nuclear cell lysates of Mec-1 variants, and the membrane was blotted with an anti-HDAC1 antibody (top) or an anti-DNMT3A antibody as internal control (bottom). A non-IP nuclear cell lysate (ncl) was used as positive control. **(H)** ChIP assay performed by IP of DNMT3A or IgG in the nuclear lysates of Mec-1 variants and amplification of *DUSP22* promoter.

Fig. 6. CLL samples with clonal NOTCH1 mutation down-modulate DUSP22 and have an increased migratory potential. (A) Distribution of the VAF in our cohort of *NOTCH1*-M CLL samples (n=113). **(B)** Pearson inverse correlation between NOTCH1-VAF and *DUSP22* levels. **(C)** qRT-PCR of *DUSP22* levels in CLL patients divided into subclonal (VAF \leq 12%, n=34) and clonal (VAF>12%, n=56) *NOTCH1*-M samples. Values are represented on a Log

scale. **(D)** Analysis of *DUSP22* expression and *NOTCH1* VAF in the follow-up of 3 CLL patients. DNA and RNA CLL samples collected at the same time were analyzed by ARMS-SYBR-PCR and qRT-PCR, respectively. **(E)** MS-PCR of *NOTCH1*-M CLL samples divided according to *DUSP22* expression. Results are represented on a log2 scale. **(F)** WB of *DUSP22* expression and STAT3 phosphorylation in *NOTCH1*-M CLL samples divided according to *DUSP22* levels. Levels of non-phosphorylated STAT3 are shown as controls. **(G)** qRT-PCR of *CCR7* expression in *NOTCH1*-M CLL samples divided according to *DUSP22* levels. Values are represented in a log2 scale. **(H)** Migration vs. CCL19 of *NOTCH1*-M CLL cells divided according to *DUSP22* levels. Values are represented in a log2 scale.

Fig. 7. Mec-1/PEST cells harbor truncating mutations in NOTCH1 PEST domain and show sustained signaling upon ligand binding. **(A)** WB analysis of NOTCH1 cleavage after co-culture on HS-5/JAG1 or /DLL1. Mec-1/WT and PEST were lysed in basal condition (-) or after 20 hours co-culture. Co-culture on mock GFP HS-5 was used as a control. Two independent PEST clones are shown. Arrows indicate WT or mutated NICD band. **(B)** WB showing the kinetic of NICD degradation after ligand withdrawal. Cells were co-cultured on HS5/DLL1 as in panel (A) and immediately lysed (0h) or removed from the HS-5 layer and lysed at the indicated time points (3, 8, 24 hours post activation). Quantification of NICD band intensity over actin band intensity is reported in **(C)**. Statistics were performed with the 2-way ANOVA test. **(D)** qRT-PCR of *HES1* expression upon NOTCH1 activation by ligand-expressing HS-5 and after ligand withdrawal. RNA was extracted at the indicated time points, *HES1* levels measured by qRT-PCR and expressed as fold change over basal levels. Statistics was performed with

the 2-way ANOVA test. **(E)** qRT-PCR analysis of *DUSP22* expression in Mec-1/WT and PEST at basal levels (-) or after co-culture on HS-5/DLL1 (+). **(F)** qRT-PCR analysis of *CCR7* expression in Mec-1/WT and PEST at basal levels (-) or after co-culture on HS-5/DLL1 (+).

Fig. 8. Mec-1 variants show different spreading *in vivo*. **(A)** MRI images of mice injected with Mec-1/WT, /KO and /PEST 3 weeks after injection. The liver and the kidneys are shown in coronal sections, and the spleen is shown in axial section. Metastatic nodules and spleens are indicated by the arrows: S, superior; I, inferior; R, right; L, left; A, anterior; P, posterior. **(B)** Kidneys' (top) and spleen's (bottom) weight in mice injected with Mec-1 variants. Pictures of the spleens are also shown. **(C)** FC analysis of Mec-1 cells (CD19⁺/CD20⁺) in the liver, spleen and brain (from left to right). **(D)** IHC of CD20⁺ areas in the spleen of mice injected with Mec-1 variants. Magnification 4X. The graph in **(E)** represents the quantification of CD20⁺ areas. **(F)** IHC of CD20⁺ areas in the brain of mice injected with Mec-1 variants. Magnification 2.5X and 4X. The graph in **(G)** represents the quantification of CD20⁺ areas.

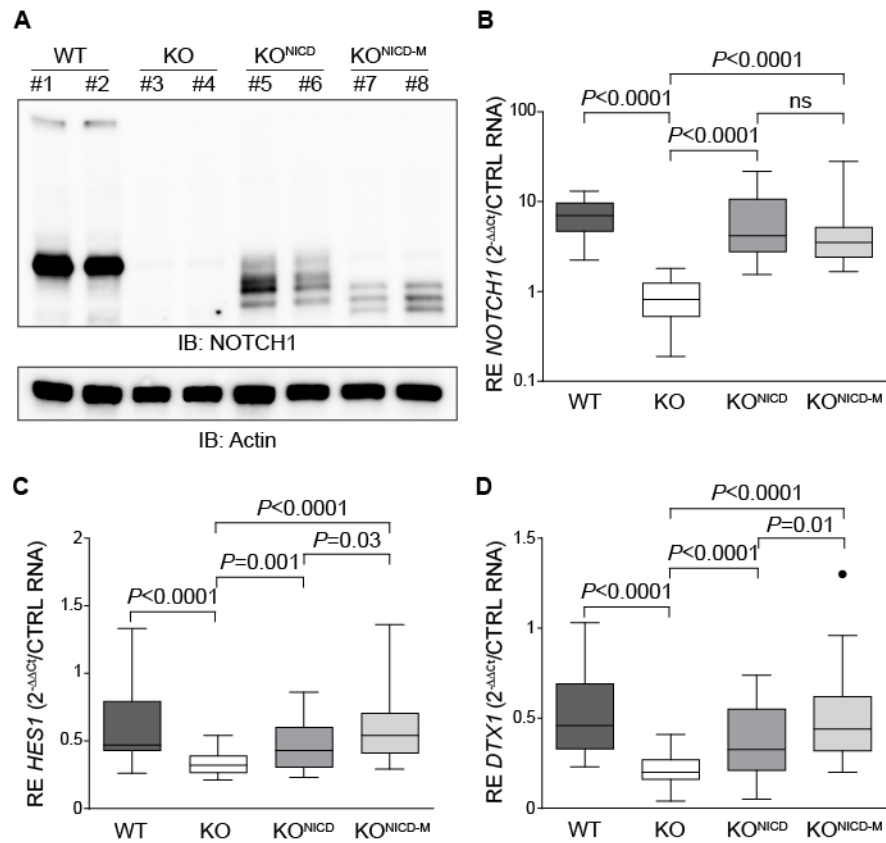


Figure 1

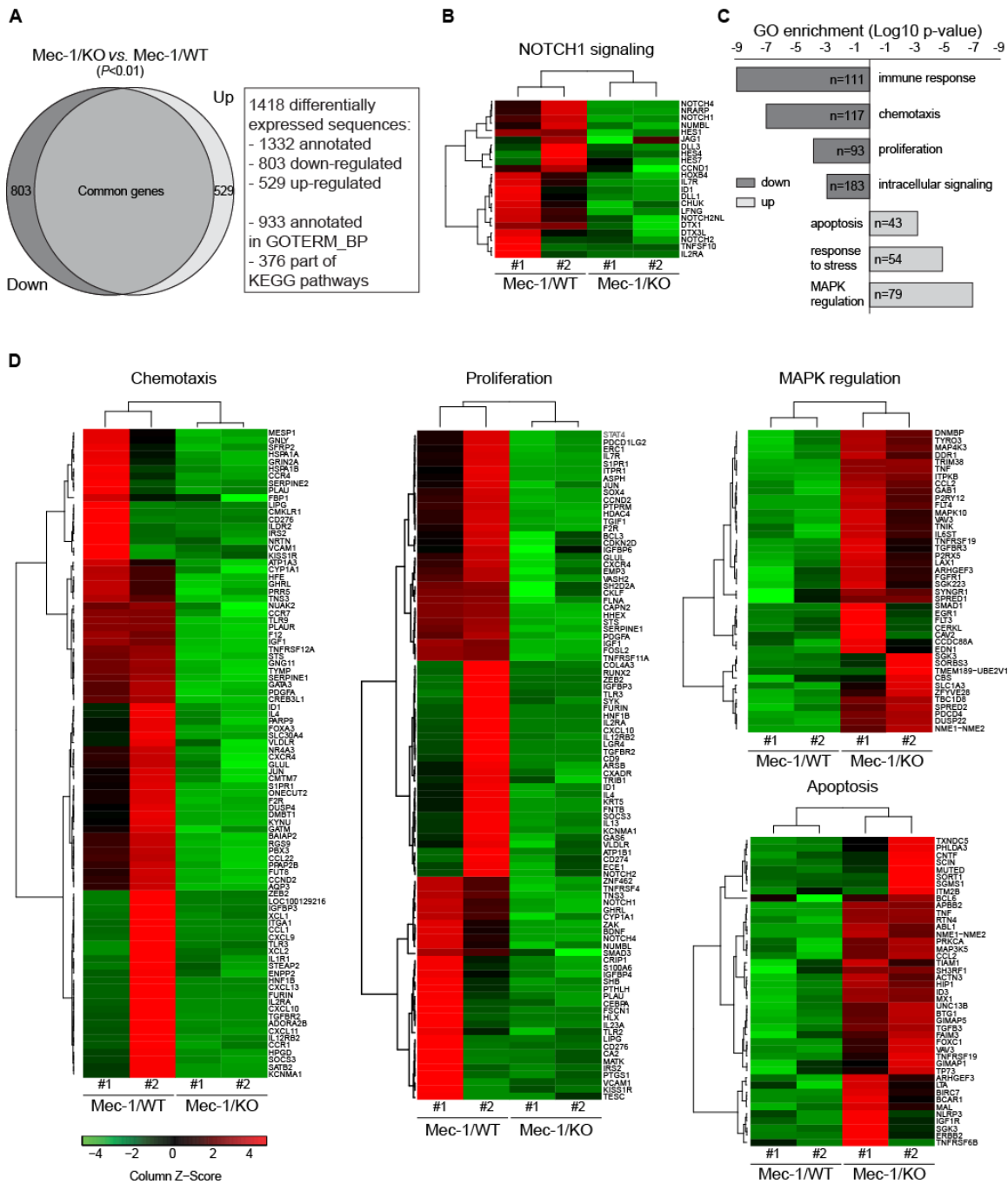


Figure 2

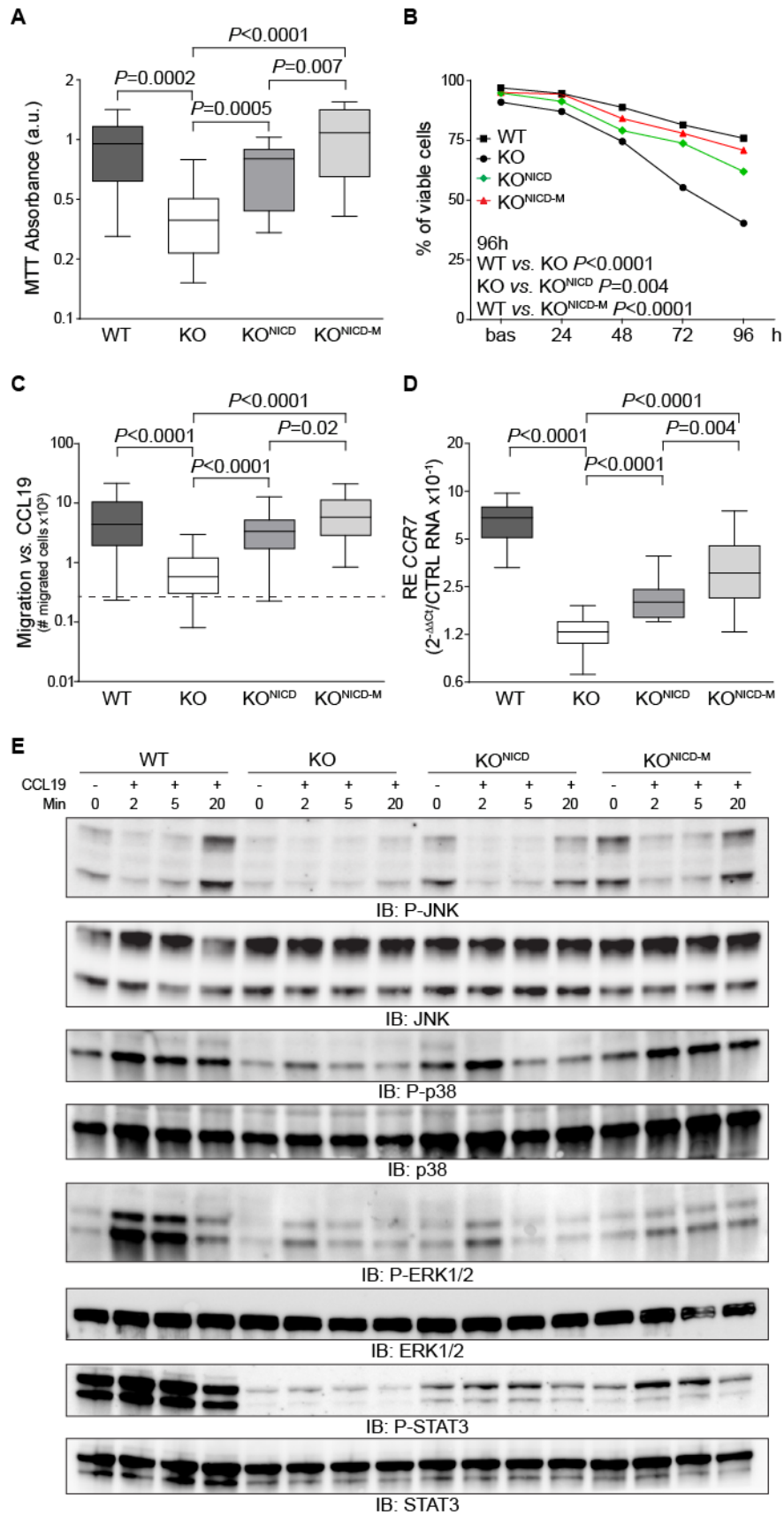


Figure 3

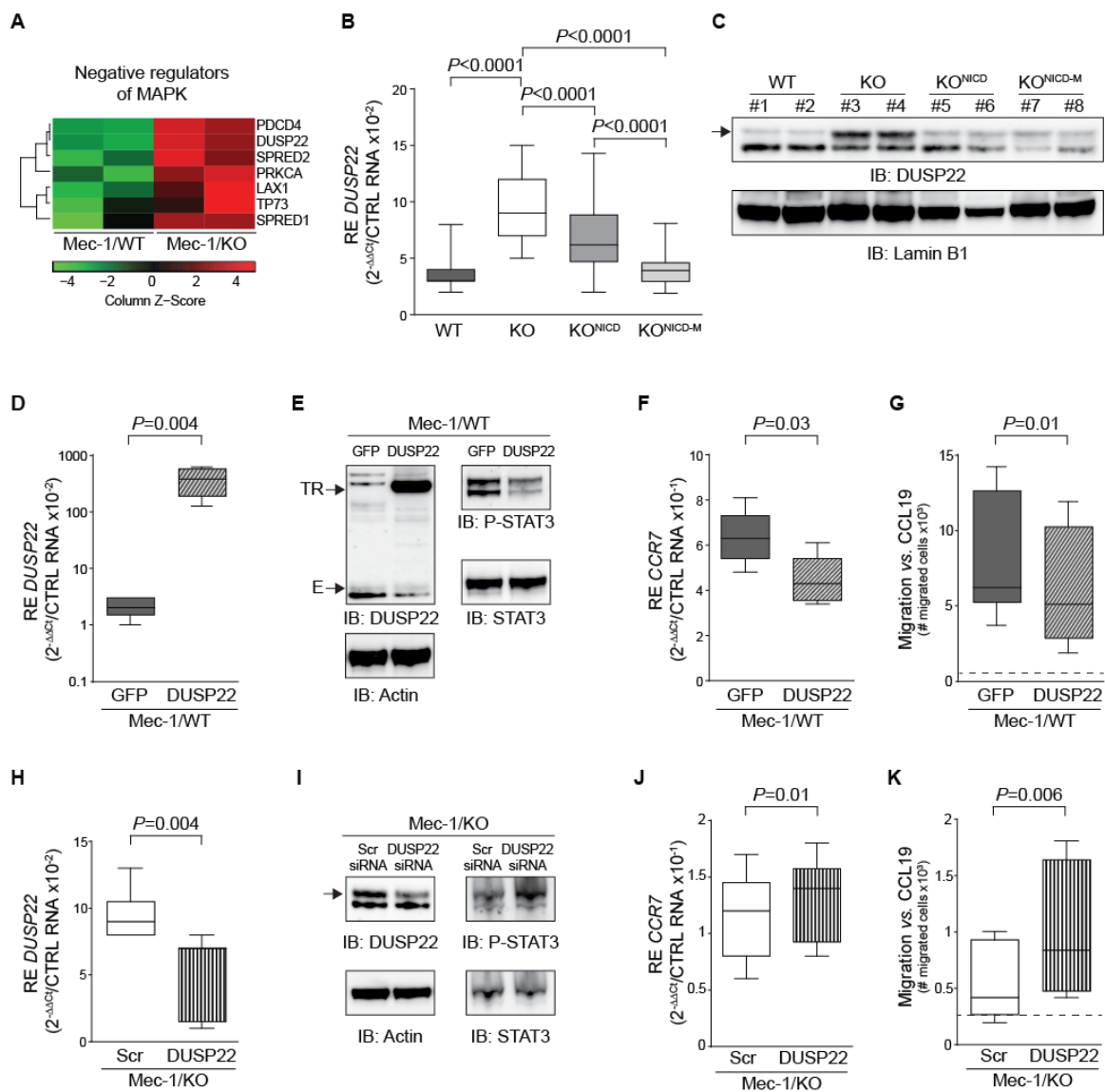


Figure 4

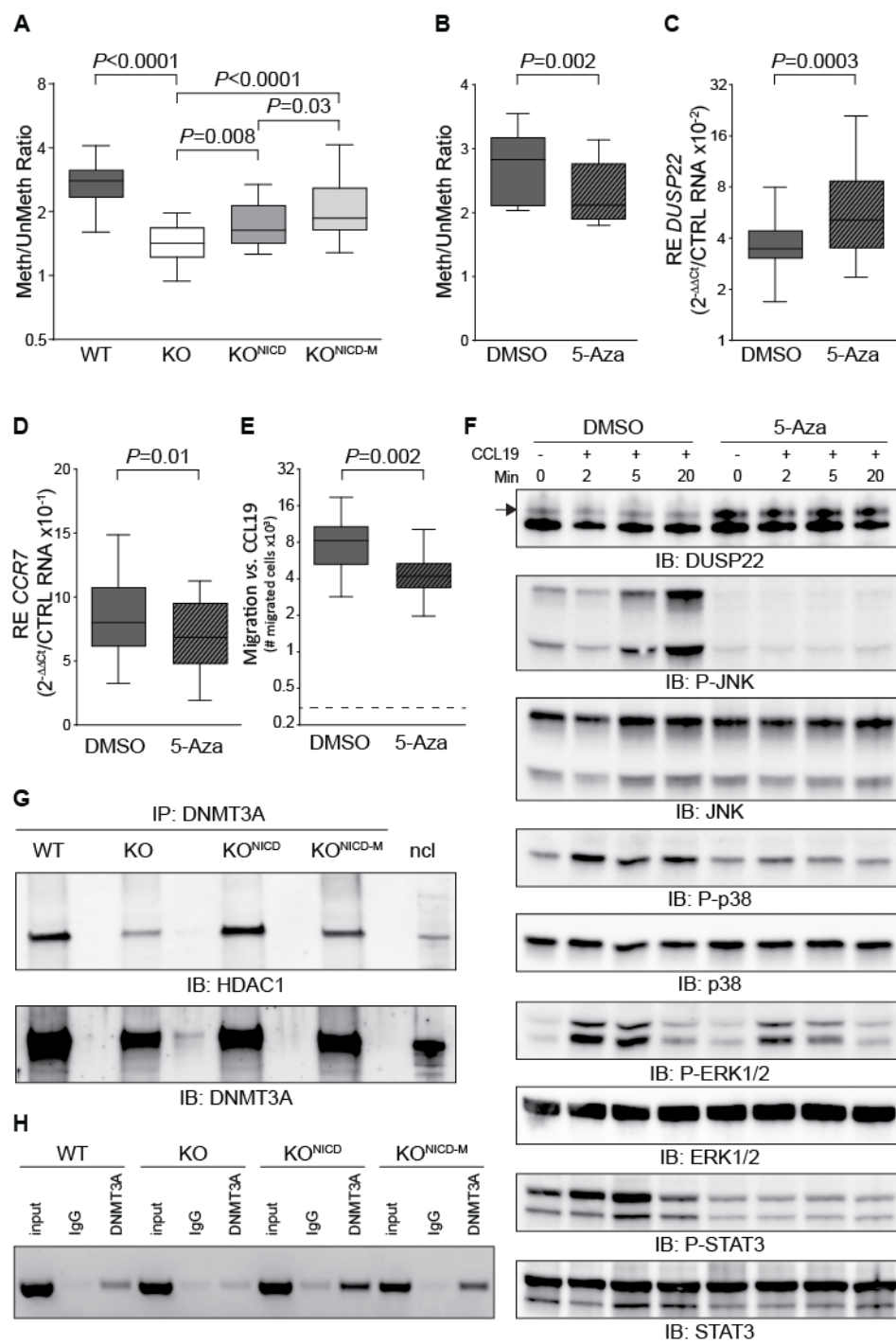


Figure 5

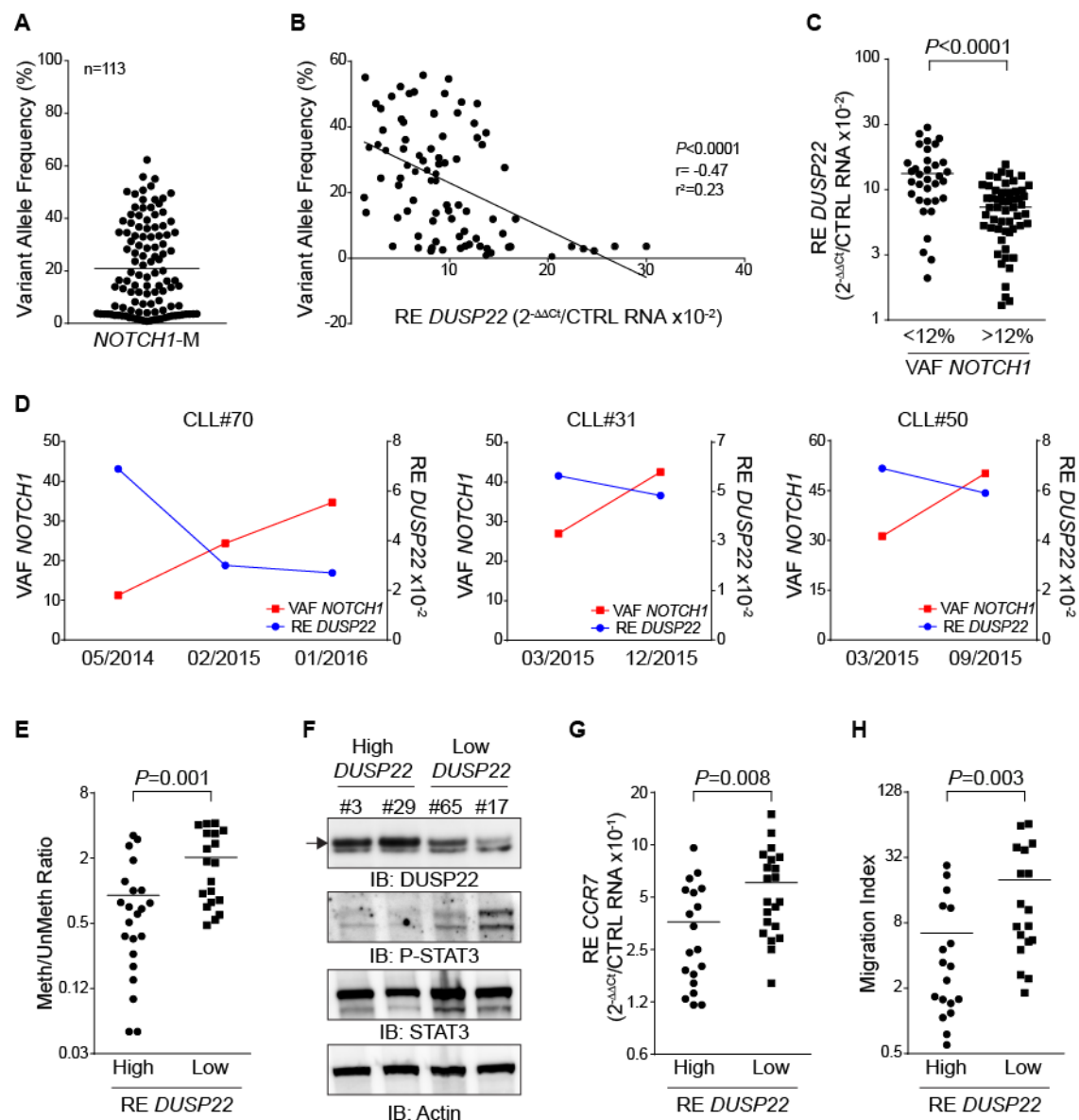


Figure 6

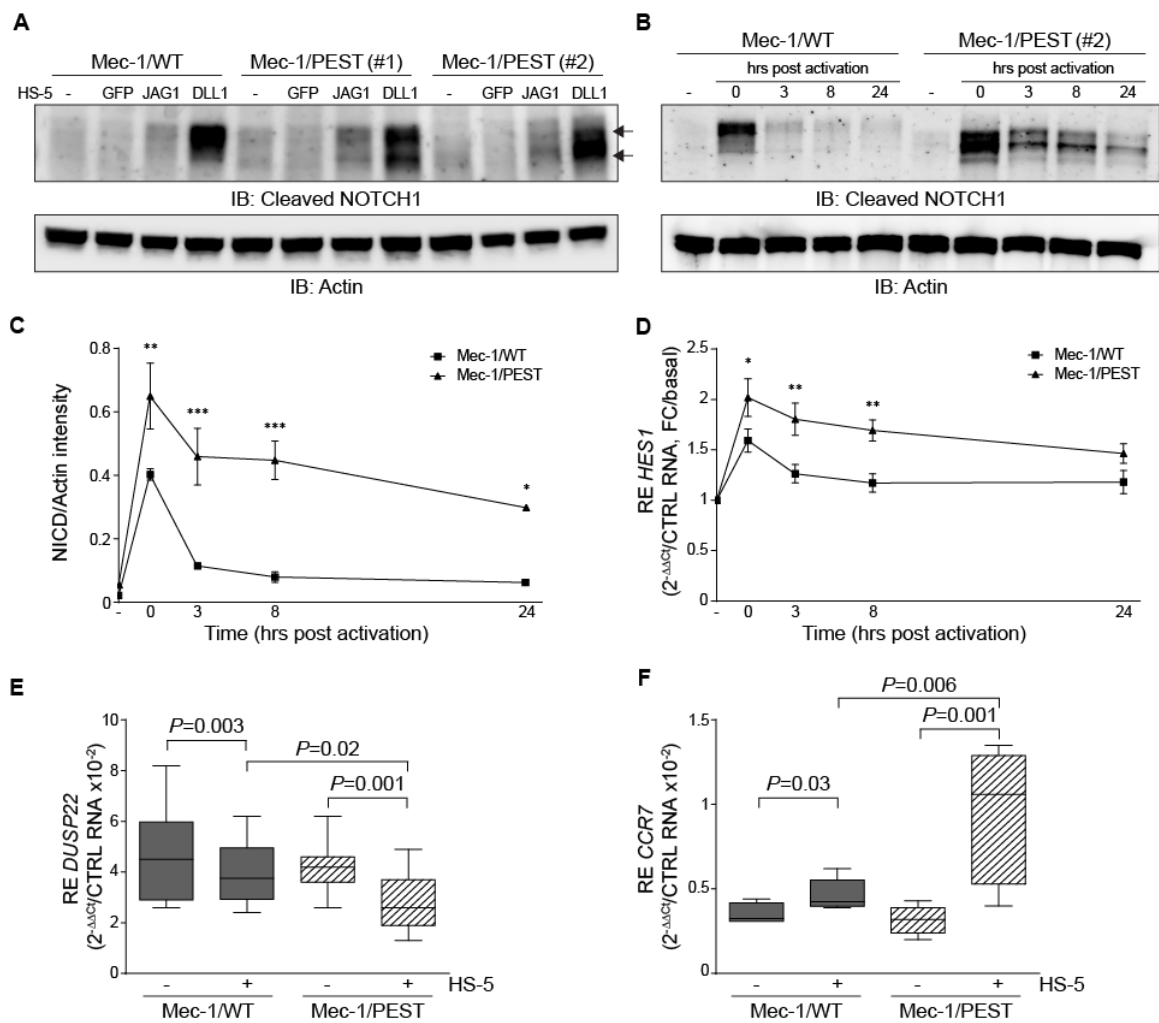


Figure 7

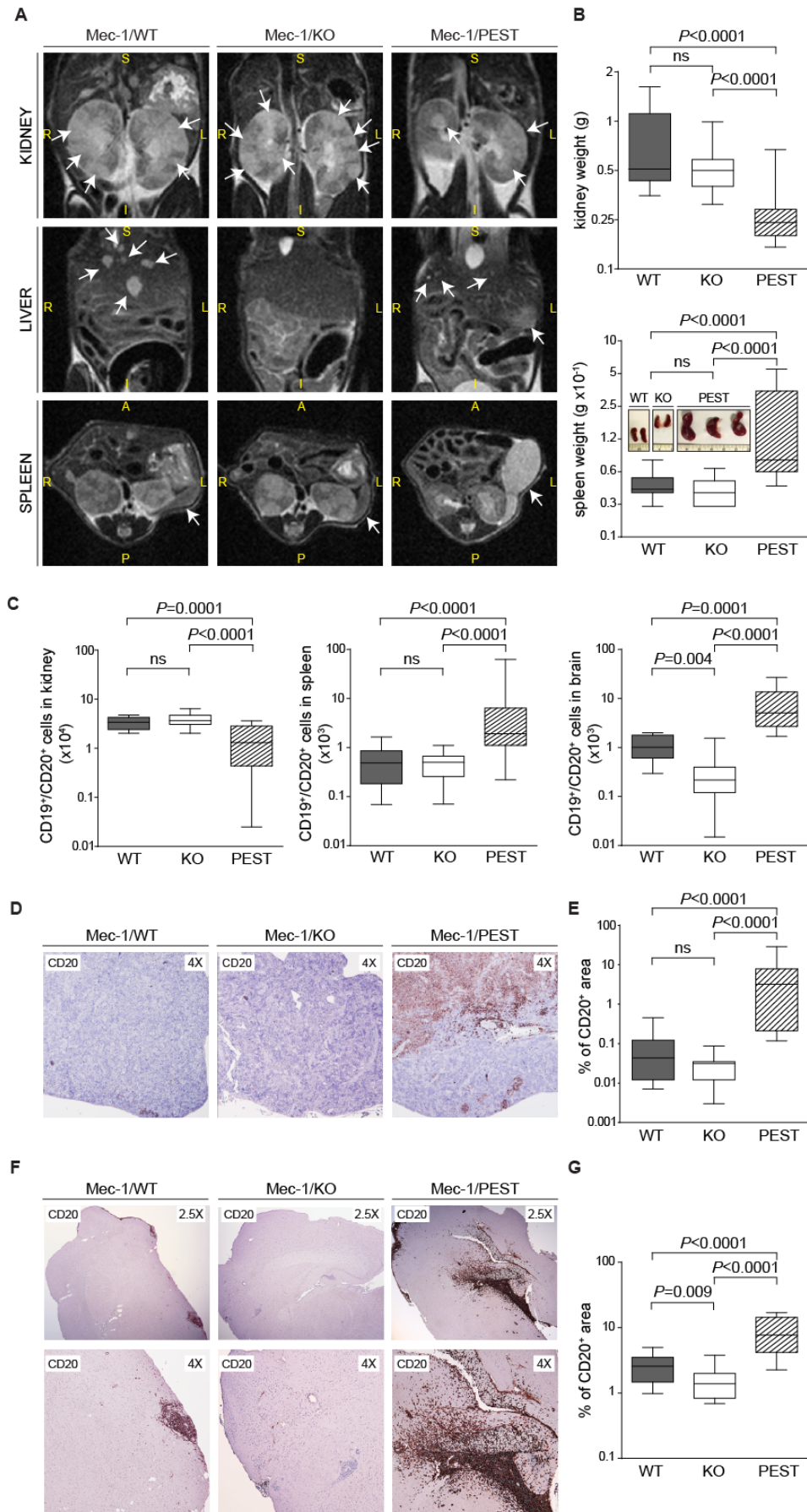


Figure 8